Military Technical College
Kobry El-Kobba
Cairo, Egypt

12-th International Conference
on
Aerospace Sciences &
Aviation Technology

EASY WAY TO DETECT AN AIRPLANE IN CASE OF HEAVY LANDING

ABOUAMER* S. A. , AL-DAHSHAN** A. S. & EL NOMROSSY*** M.

ABSTRACT

In this report, the piezoelectric materials are used to detect heavy landing (touch-down) conditions through a group of sensors assembled within the main landing gear system. Outlines about piezoelectric materials and it's technical characteristics are included. Measurement procedures have been held and pointed out in a previous work. Mathematical Analysis & Modeling of Piezoelectrics sensors integrated to the host mechanical structure are also introduced. A comparison between the analytical results and some experimental ones from other work were done successfully. Analytical power estimation to obtain maximum output voltage from these sensors was discussed. Design control procedures using the optimum coordination approach in time domain is recommended.

KEY WORDS

Smart Structure, Piezoelectric Material, and Aircraft Landing Gear.

* Vice Dean of AHI for management & Informatics
** Chairman of AHI for management & Informatics
*** Chairman of Arab Organization Research Center

I. Introduction

The function of materials for Aircraft structure has been progressed by the application of materials with improved strength, stiffness, and light weight characteristics.. Smart material systems and structures can highly contribute to those objectives. Two major areas can be identified. The first one is for the health monitoring systems which are able to detect localize and validate deterioration due to fatigue, corrosion, impact, mishandling, wear, temperature, or any other environmental conditions of the Aircraft structures, engines, systems, and equipments. The second one is for the active structures which are applied to cabin noise reduction, vibration and flutter suppression of engines, wings, and fins, variation in wing profiles and geometries for optimized aerodynamical behavior and maneuvers.

Nowadays a common method used to analyze the health status of composite structure is to mount a series of piezoelectric (sensors) onto its surfaces. These sensors are used to detect the vibration patterns emitted from the structure. Vibrations cause these sensors to generate a very small electrical current, which can then be recorded into a computer. Any abnormal patterns can be detected by the comparison with the stored normal spectrum patterns; consequently the health of the structure can be determined based on the comparison.

In the field of light weight trainer aircraft due to less experience of the trainee pilot it happens many times that the landing forces exceed the limits, causing what is called (heavy landing at touchdown). In fact, the most critical loads on the landing gear occur at high gross weight and high rate of descent at touch down. Since the landing gear has requirements of static strength and fatigue strength similar to any other component, overstress must be avoided to prevent failure and derive the anticipated service life from the components.

In this work, piezoelectric material is used as a sensor device to detect heavy landing. This is done by using sensors made of piezoelectric material within the landing gear shock absorber internal cavity and connects their poles through cables to a volt measuring device, which record the value of the induced volt with relation to the force of impact due to heavy landing at touchdown. During design the system must be considered to satisfy the airworthiness requirements which include all certification requirements and passing all types of static, dynamic, and functional tests at all specified environmental conditions.

Finding a more precise and predictive model of power harvesting is the objective of this work. Methods of modeling piezoelectric materials in conjunction with host structure will be used to generate maximum values of power produced from the impact forces due to landing inside shock absorber see Fig. 1. This optimum produced power can be doubled or increased multiple of times the value obtained from a single beam model one by increasing number of beams supporting the sensing device (simple stack piezoelectric transformer). In fact the most recommended target is to obtain maximum output power with minimum weight and complexity.

II. Smart Structure System with Piezoelectric materials

The intelligent system consists of one or more microprocessors that analyze the responses from the sensors and use integrated control theory to command the actuators to apply localized strains/displacements to alter system response. A smart structure has the capability to respond to the external environmental changes (such as loads or shape change) as well as to the internal environment changes (such as damage or failure). It incorporates the smart material actuators that allow the alteration

of system characteristics (such as stiffness or damping) as well as of system response (such as strain or shape) in a controlled manner. In fact a smart structure involves four key elements: actuators, sensors, control strategies, and power conditioning electronics Fig. 2.

Smart structures are basically classified into two main types which are Ref [18]:

1- Passive smart structure: it contains a built in sensing device to continuously monitor the current state and serviceability of the structure. These allow us to have a clear view of how far away from failure a particular structure is.

2- Active smart structure: it has embedded sensors to monitor and measure the performance of the structure, then it has the ability to compare the measured data with a certain specified values and has the means of control to perform the corrective action through an embedded actuators.

III. Piezoelectric Materials Characteristics

The piezoelectric effect relates mechanical effects to electrical effects. These effects are highly dependent upon their orientation to the poled axis. It is, therefore, essential to maintain a constant axis numbering scheme, see Fig. 3. All materials, regardless of their relative hardness, follow the fundamental law of elasticity. The elastic properties of the piezoelectric material control how well it will work in particular application. The relationship between stress and strain is Hooke's Law which can be expressed as:

$$\sigma = E\,\varepsilon \qquad \text{(III.1)}$$

Or $\varepsilon = S\,\sigma$ for isotropic materials where $S = 1/E$ (III.2)

And $\sigma_i = E_{ij}\,\varepsilon_j$ (III.3)

Or $\varepsilon_i = S_{ij}\,\sigma_j$ for anisotropic materials (III.4)

Fortunately, many of the constants in the formulas above are equal to zero for PZT piezoelectric ceramics. The non-zero constants are,

$$S_{11},\ S_{22},\ S_{33},\ S_{12},\ S_{13},\ S_{23},\ S_{44}, \text{ and } S_{66}$$

with $S_{11} = S_{22}$

and $S_{66} = 2\,(S_{11} + S_{12})$

$$[S] = \begin{bmatrix} S_{11} & S_{12} & S_{13} & 0 & 0 & 0 \\ 0 & S_{22} & S_{23} & 0 & 0 & 0 \\ 0 & 0 & S_{33} & 0 & 0 & 0 \\ 0 & 0 & 0 & S_{44} & 0 & 0 \\ 0 & 0 & 0 & 0 & 0 & 0 \\ 0 & 0 & 0 & 0 & 0 & S_{66} \end{bmatrix} \qquad \text{(III.5)}$$

Where, superscripts describe external factors (physical mounting, electrical conditions, etc.) that effect the piezoelectric property, while subscript describe the relationship of the property to the poling axis.

The characteristics of piezoelectric properties depend on their orientation to the poling axis. This orientation determines the direction of the action or response associated with the property. Example:

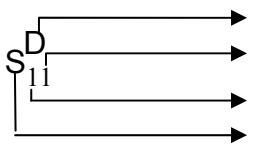

Indicates that compliance is measured with electrode circuit

Indicates that <u>stress</u> or strain is in direction of axis 1

Indicates that <u>strain</u> or stress is in direction of axis 1

Compliance = strain / stress (S = 1 / E)

Coupling is a key constant used to evaluate the "quality" of an electro-mechanical material. This constant (Electro Mechanical coupling Coefficient k) represents the efficiency of energy conversion from electrical to mechanical or mechanical to electrical Ref [3].

$$k^2 = \frac{\text{M. E. Converted to E. Charge}}{\text{M. E. Input}} \quad \text{or} \quad = \frac{\text{E. E. Converted to M. Displacement}}{\text{E. E. Input}} \qquad \text{(III.6)}$$

IV. Piezoelectric benders

Piezoelectric benders are often used to create actuators with large displacement capabilities. The benders work in a mode which is very similar to the action of a bimetallic spring. Two separate bars or wafers of piezoelectric material are metallized and poled in the thickness expansion mode. They are then assembled in a + - + - stack and mechanically bonded. In some cases, a thin membrane is placed between the two wafers.

The outer electrodes are connected together and a field is applied between the inner and outer electrodes. The result is that for one wafer the field is in the same direction as the poling voltage while the other is opposite to the poling direction. This means that one wafer is increasing in thickness and decreasing in length while the other wafer is decreasing in thickness and increasing in length, resulting in a bending moment as shown in Fig. 4. There are two sources for loss in a piezoelectric device. One is mechanical and the other is electrical.

The piezoelectric element can be represented by the simple model given in Fig. 5, where:

R_i Electrical Resistance
C_i Input capacitance = $\varepsilon_o \varepsilon_r A / t$
ε_o dielectric constant of air = 8.85×10^{-12} farad/meter
A Electrode Area
T Dielectric Thickness
L_M Mass (Kg)
C_M Mechanical Compliance = 1 / Spring Rate (M/N)
N Electro-mechanical Linear Transducer Ratio (Newton/volt or coulomb /meter)

This model has been simplified and it is missing several factors. It is only valid up to and slightly beyond resonance.

1- The model is related to the mechanical compliance (C_M).
2- The resistance due to mechanical Q_M has been left out.
3- There are many resonant modes in the transformers, each of which has its own C_M see Fig 6.

V. Simple Stack Piezoelectric Transformer

The piezoelectric Transformer acts as an ideal tool to explain the modeling of piezoelectric devices in that it utilizes both the direct and indirect piezoelectric effects. The transformer operates by first converting electrical energy into mechanical energy in one half of the transformer. This energy is in the form of a vibration at the acoustic resonance of the device. The mechanical energy produced is then mechanically coupled into the second half of the transformer. The second half of the transformer then reconverts the mechanical energy into electrical energy. The transformer is driven across the lower half (dimension d1) resulting in a thickness mode vibration. This

vibration is coupled into the upper half and the output voltage is taken across the thinner dimension d_2. In Fig. 7, the basic layout of a stack transformer is shown.
The equivalent circuit model for the transformer, see Fig. 8, can be thought of as two piezoelectric elements that are assembled back to back. These devices are connected together by an ideal transformer representing the mechanical coupling between the upper and lower halves. The input resistance, R_i, and the output resistance, R_o, are generally very large and have been left out in this model. The resistor R_L represents the applied load. The values of various components can be calculated as shown previously.

1- Input / Output Capacitance

$$C_i = \varepsilon_o \varepsilon_r \frac{\text{Input Area}}{\text{Input Thickness}} = \varepsilon_o \varepsilon_r \frac{L.\,W}{d_1} \qquad (V.1)$$

Similarly

$$C_o = \varepsilon_o \varepsilon_r \frac{\text{Output Area}}{\text{Output Thickness}} = \varepsilon_o \varepsilon_r \frac{n.\,L.\,W}{d_1} \qquad (V.2)$$

2- Mechanical Compliance:
The mechanical compliance can be represented by a simple beam subjected to a uniform distributed axial load. This is because the thickness expansion mode will apply uniform stress across the surface. It should be noted that the beam length is measured with respect to the vibration node. The vibration node is used as this is the surface which does not move at resonance and can be considered as a fixed mounting surface.

Thus $C_{M1} = \frac{d_1}{LW\ E_{33}}$ and $C_{M2} = \frac{d_2}{LW\ E_{33}}$ (V.3)

Note: even if $n.d_2 \neq d_1$ the vibration node will still be located in the mechanical center of the transformer.

3- Mass

$$L_{M1} = \rho\, L\, W\, d_1 \quad \text{and } L_{M2} = \rho\, L\, W\, n\, d_2 = \rho\, L\, W\, d_1 \qquad (V.4)$$

4- Resistance
The resistance in the model is a function of the mechanical loss Q_M and Q of the material at resonance and will be calculated later*.

5- Ideal Transformer Ratio
The transformer ratio, N_1, can be thought of as the ratio of electrical energy input to the resulting ratio of electrical energy input to the resulting mechanical energy output. This term will then take the form of Newton per volt and can be derived from the piezoelectric constant, g, where,

$$g = \frac{\text{Electric Field}}{\text{Stress}} = \frac{\text{Volts / Meter}}{\text{Newton / Meter}^2} \qquad (V.5)$$

Therefore: $\frac{1}{g} = \frac{N / m^2}{V / m}$

$$N_1 = \frac{1}{g} \frac{\text{Area of Applied Force}}{\text{Length of Generated Field}} = \frac{L.\,W}{g_{33}.\,d_1} \qquad (V.6)$$

The output section converts mechanical energy back to electrical energy and the ratio would normal be calculated in an inverse fashion to N_1. In the model, however, the transformer ratio is shown as N_2:1. This results in a calculation for N_2 that is identical to the calculation of N_1.

$$N_2 = \frac{1}{g} \frac{\text{Area of Applied Force}}{\text{Length of Generated Field}} = \frac{L.\,W}{g_{33}.\,d_2} \qquad (V.7)$$

The transformer 1:N_c, represents the mechanical coupling between the two halves of the transformer. The stack transformer is tightly coupled and the directions of stress are the same in both halves. This results in $N_c = 1$.
The response of the transformer can be calculated from this model, but it is possible to simplify the model through a series of simple network conversion and end up in an equivalent circuit whose form is the same as that of a standard magnetic transformer, see Fig. 9. Where, due to translation through the transformer,

$$C_{M2}` = N_c^2\, C_{M2} \quad \text{and} \quad L_{M2}` = L_{M2} / N_c^2 \qquad (V.8)$$

But $N_c^2 = 1$, therefore $C_{M2}` = C_{M2} = C_{M1}$ and $L_{M2}` = L_{M2} = L_{M1}$ (V.9)

Thus the next level of simplification will be, see Fig. 10.

Where, $L` = L_{M1} + L_{M2}` = 2\,L_1 = 2\,r\,.\,L\,.\,W\,.\,D_1$ (V.10)

$$C` = \frac{C_{M1}\,C_{M2}`}{C_{M1} + C_{M2}`} = \frac{C_{M1}^2}{2\,C_{M1}} = \frac{C_{M1}}{2} \frac{d_1}{2.L.W.E_{33}} \qquad (V.11)$$

And the final simplification, see Fig. 11, will be:

$$C = C`\,N_{12} \quad \text{and} \quad L = L` / N_{12} \qquad (V.12)$$

Therefore:

$$N_1 = \frac{L.W}{g_{33}.d_1} \qquad (V.13)$$

$$C = C`.\,N_1^2 = \frac{d_1}{2.L.W.E_{33}} \left\{ \frac{L.W^2}{g_{33}.d_1} \right\} = \frac{L.W}{2E_{33}\,g_{33}^2.d_1} \qquad (V.14)$$

$$L = 2.\,\rho.L.W.d_1 \left\{ \frac{g_{33}.d_1}{L.W} \right\}^2 = \frac{2.\rho\,.g_{33}^2.d_1^3}{L.W} \qquad (V.15)$$

$$N = \frac{N_1\,N_C}{N_2} = \frac{L\,.\,W}{g_{33}\,.\,d_1} \frac{g_{33}\,.\,d_2}{L\,.\,W} = \frac{d_2}{d_1} \qquad (V.16)$$

The last value to be calculated is the motional resistance. This value is based upon the mechanical loss Q_M of the material and the acoustic resonant frequency where,

$$\omega_o = 1 / \sqrt{L.C} = 1 / \sqrt{\frac{2.\,\rho\,.g_{33}^2.d_1^3}{L.W} \frac{L.W}{2E_{33}\,g_{33}^2.d_1}} \qquad (V.17)$$

$$= 1 / \sqrt{\rho.d_{12} / E_{33}} = 1 / \left\{ d_1 \sqrt{\rho / E_{33}} \right\} \qquad (V.18)$$

The speed of sound in PZT is $C_{PZT} = E / \rho$

Therefore $\omega_o = C_{PZT} / d_1$ (V.19)

Equation (V.19) states that the resonant frequency is equal to the speed of sound in the material divided by the acoustic length of the device. This is the definition of acoustic resonance and acts as a good check of the model. *The resistance is then derived as follows:

Since $Q_M = 1 / \omega_o.R.C \Longrightarrow R = 1 / \omega_o.Q_M.C$ (V.20)

Therefore $R = 1 / d_1 \left\{ \sqrt{\rho / Y_{33}} \right\} \left\{ Q_M \right\} \left\{ L.W / 2E_{33}\, g_{33}^2.d_1 \right\}$ (V.21)

$$= \left\{ 2\, d_1^2\, g_{33}^2 \sqrt{\rho\, Y_{33}} \right\} \Big/ \left\{ Q_M\, L.W \right\} \quad \text{(V.22)}$$

Note that C_M and R are both functions of Y_{33} and Y_{33} is a function of R_L.
It should be noted that the model is only valid for transformers driven at or near their fundamental resonate frequencies. This is because the initial mechanical model assumed a single vibration node located at the center of the stack, which is only true when the transformer is driven at fundamental resonance. There are more nodes when the transformer is driven at harmonic frequencies as shown in Fig. 13. Note that the stress is 90^o out of phase from displacement. There are no fixed nodes at frequencies other than resonance. This means that the transformer must be designed with the resonance mode in mind otherwise phase cancellations will occur and there will be little or no voltage gain.

VI. Modeling of Piezoelectric Material on a Beam

In the following a three analytical methods for modeling a unimorph cantilever beam are used.

1. Pin-force method

The pin-force model describes the mechanical interaction between the piezoelectric and the substrate elements. Pins connect the two elements at the extreme ends of the PZT. Perfect bonding between the two elements is implied, and the adhesive layer is infinitely stiff. Shear stress in the piezoelectric is concentrated only in a small area at the pin ends. The strain in the beam is assumed to follow Euler-Bernoulli beam theory where the strain increases linearly through the thickness. Though the strain in piezoelectric is assumed to be constant through the thickness. Because of this constant strain, the pin-force method does not take into account the bending stiffness of the piezoelectric patches, and the method is limited when the stiffness of the substrate becomes approximately five times larger than the piezo stiffness. Fig. 14, shows the pin-force model strain state for a unimorph bender. The PZT is attached to the top of a thin beam. When the substrate and piezoelectric material are subjected to an external moment, the PZT strain ε_p can be written as:

$$\varepsilon_p = \sigma_p / E_p \quad \text{(VI.1)}$$

$$\varepsilon_p = F / E_p .b.\, t_p \quad \text{(VI.2)}$$

The strain on the beam is modeled as:

$$\varepsilon_b = -(t_b / 2).\, K \quad \text{(VI.3)}$$

The equation for the external moment applied to the beam is:

$$M_p = M - F\,(t_b/2) = (E_b\,.\,I_b)k \qquad \text{(VI.4)}$$

From (VI.2) and (VI.3), the beam curvature will be:

$$k = -\,2F/E_p.b.t_p.t_b \qquad \text{(VI.5)}$$

Substituting equation (VI.5) into (VI.4) gives

$$F = 6\,E_p.t_p.M\,/\,(3\,E_p.t_p.t_b - E_b.t_b^2) \qquad \text{(VI.6)}$$

Combining Equations (VI.2) and (VI.6) lead to a strain expression on the interface as:

$$\varepsilon_p = 6\,M\,/\,b.(3\,E_p.t_p.t_b - E_b.t_b^2) \qquad \text{(VI.7)}$$

Since the stress is $\sigma_p = E_p\,\varepsilon_p$, therefore:

$$\sigma_p = 6\,E_p\,.M/b.(3\,E_p.t_p.t_b - E_b.t_b^2) \qquad \text{(VI.8)}$$

The voltage on the PZT poling surfaces is related to the stress by:

$$V = g_{31}.t_p.\sigma_p \qquad \text{(VI.9)}$$

Where, g_{31} is the PZT voltage constant. The voltage is related to the moment by substituting (VI.8) into (VI.9)

$$V = 6.g_{31}.M\,/\,b.t_b\,(3 - \Psi) \qquad \text{(VI.10)}$$

where $$\Psi = E_b.t_b\,/\,E_p.t_p \qquad \text{(VI.11)}$$

2- Enhanced pin-force method

The enhanced pin-force model expands upon the pin-force model by taking into consideration the PZT bending stiffness. The strain does not remain constant as in the pin-force model but increase linearly through the PZT thickness, as shown in Fig. 15.

A drawback still exists when using this method, because the PZT is assumed to bend on its own neutral axis. This assumption basically treats the PZT and substrate as two separate structures connected only by the end pins. In this case the moment acting on the beam is:

$$M_b = M - F(t_b/2) - M_b = (E_b\,I_b)k \qquad \text{(VI.12)}$$

Where $M_b = M_p = (E_b.I_b)k$

From (VI.2) and (VI.3), it is found that:

$$F = -\,(E_p.b.t_p.t_b\,/2).k \qquad \text{(VI.13)}$$

Combining Equations (VI.12) and (VI.13), the curvature will:

$$k = 12.M/\{-6\,E_p.b.t_p.t_b^2 + E_p.b.t_p^3 + E_b.b.t_b^3\} \qquad \text{(VI.14)}$$

Substituting Equation (VI.14) into (VI.13) and then into (VI.2), gives an expression for strain as:

$$\varepsilon_p = 6.t_b.M/\{6\,E_p.b.t_p.t_b^2 - E_p.b.t_p^3 - E_b.b.t_b^3\} \qquad \text{(VI.15)}$$

Te stress will be:

$$\sigma_p = 6.t_b.E_p.M/\{3E_p.b.t_p.t_b^2 - E_{\,p}.b.t_p^3 - E_b.b.t_b^3\} \qquad \text{(VI.16)}$$

Finally substituting equation (VI.16) into (VI.9) and then into (VI.10) (with $T=t_b/t_p$) leads to the voltage as:

$$V = 6\, g_{31}\, .T.M \,/\, b.t_b\, (3T^2 - 1 - \Psi T^2) \qquad \text{(VI.17)}$$

3- Euler-Bernoulli method

In the Euler-Bernoulli model the PZT and substrate both bend about a common neutral axis which is no longer the neutral axis of the beam shown in Fig. 16-a. This neutral axis is calculated by the modulus-weighted algorithm see Fig. 16-b. The equation for the distance to the neutral axis can be written as:

$$Z_s = \frac{\sum_{i=1}^{n} z_i \frac{E_i}{E_r} A_i}{\sum_{i=1}^{n} \frac{E_i}{E_r} A_i} = \frac{\left\{\frac{t_p}{2}\, t_p \frac{E_p}{E_b}\right\} + \left\{t_p + \frac{t_b}{2}\right\}. t_b}{t_p \frac{E_p}{E_b} + t_b} \qquad \text{(VI.18)}$$

To simplify the calculations the average strain in the PZT is determined and used to find the voltage. The average strain is:

$$\varepsilon_p = - M (z_s - t_p/2) \,/\, \{E_p I_p + E_b I_b\} \qquad \text{(VI.19)}$$

With:

$$I_p = \int_{z_s - t_p}^{z_s} b\, z^2\, dz = (1/3)\, b\, \{z_s^{\,3} - (z_s - t_p)^3\} \qquad \text{(VI.20)}$$

$$I_b = \int_{-(t_p + t_b - z_s)}^{z_s - t_p} b\, z^2\, dz = (1/3)\, b\, \{(t_p + t_b - z_s)^3 - (z_s - t_p)^3\} \qquad \text{(VI.21)}$$

Substituting equation (VI.17), after substituting (VI.19) and (VI.20), into (VI.18) gives:

$$V = \frac{- 6.g_{31}\, M.\, \Psi\, (1+T)}{b.t_p\, \{1 + \Psi^2.T^2 + 2.\, \Psi\, (2 + 3.T + 2.T^2)\}} \qquad \text{(VI.22)}$$

Matching the external load impedance with the internal PZT impedance will assure maximum power output. The relationship between power and resistance, which is derived for purely resistive circuit as:

$$P = \bar{V}_S^{\,2}\, R_L \,/\, (R_S + R_L)^2 \qquad \text{(VI.24)}$$

Where V_S is the RMS source voltage value in phasor notation, R_L and R_S are the resistance values for the load and source, respectively. It is evident that the maximum power is produced when $R_L = R_S$.

The Euler-Bernoulli definition of a beam, "length is over ten times larger than width". The PZT is attached to the beam near the clamped edge for maximum strain. Power estimation from PZT due to beam vibration can be determined based on the moment that the PZT experiences. This moment can be evaluated by solving for the deflection of the beam and then estimating the experienced moment as a function of the beam's curvature. The governing equation of the beam is:

$$\rho A \frac{\partial^4 w(x,t)}{\partial t^4} + E_b I_b \frac{\partial^4 w(x,t)}{\partial x^4} = F(t) \qquad \text{(VI.25)}$$

Where w is the lateral displacement of the beam, F(t) is the external applied force, ρ is density, and A is its cross-sectional area. Power generator actuated by harmonic is used to drive the system as shown in Fig. 12. When the driving force is harmonic one, equation (VI.25) will be:

$$\frac{\partial^4 w(x,t)}{\partial t^4} + c^2 \frac{\partial^4 w(x,t)}{\partial x^4} = (F_o/\rho A) \sin(\omega t)\, d(x-L_f) \qquad \text{(VI.26)}$$

Where ω is the driving frequency, Lf is the position of the applied force from the clamped edge, and $C^2 = (E_b I_b / \rho A)$. The driving frequency will be equal to the beam's first natural frequency because the largest deflection occurs at the first natural frequency.The solution of equation (VI.26) will take the form:

$$w(x,t) = \sum q_i(t).X_i(x) \qquad \text{(VI.27)}$$

Where q_i is the i^{th} modal coordinate equation of the beam, and X_i is the i^{-th} mode shape of the beam. For consistency, only the first three mode shapes will be used, The general mode shape equation for a cantilever beam is found to be:

$$X_i(x) = \cosh(\beta_i x)-\cos(\beta_i x) - \frac{\sinh(\beta_i L_b)-\sin(\beta_i L_b)}{\cosh(\beta_i L_b)+\cos(\beta_i L_b)} \{\sinh(\beta_i x)-\sin(\beta_i x)\} \qquad \text{(VI.28)}$$

Where L_b is the beam length, $\beta_i^4 = \omega_{ni}^2/c^2$, and ω_{ni} the i^{-th} natural frequency, which is found from the characteristic equation, (The result is shown in Fig. 17, and Table 1.)

$$\cos(\beta_i L_b)\cosh(\beta_i L_b) = -1 \qquad \text{(VI.29)}$$

Using orthogonality, the external force can be simplified to the expression:

$$F_i(t) = (F_o / \rho A) \sin(\omega t)\, X_i(L_f) \qquad \text{(VI.30)}$$

The convolution integral for any arbitrary input to evaluate q_i is in the form:

$$q_i(t) = (1/\omega_{di})\, e^{-\xi \omega_{ni} \tau} \int_0^t F_i(\tau)\, e^{-\xi \omega_{ni} \tau} \sin(\omega_{di}(t-\tau))\, d\tau \qquad \text{(VI.31)}$$

Where, ω_d is the damped natural frequency, and, ξ is the damping ratio (The most common damping ratio values fall between 0.01 and 0.05). For simplicity, the average value (ξ = 0.03) were used see Ref. [6]. Equations (VI.28) and (31) are used to evaluate equation (VI.27). Next we calculate the beam curvature as:

$$\kappa(x,t) = \partial^2 w(x,t) / \partial x^2 \qquad \text{(VI.32)}$$

To eliminate the dependence of length, the average curvature was evaluated as:

$$\overline{\kappa}(t) = (1/L_p) \int_0^{L_p} \kappa\,(x,t)\, dx \qquad \text{(VI.33)}$$

The limits of integration are the lengths along the beam where the PZT starts and ends, See Fig. 18-a, and 18-b. The applied moment acting on the beam is:

$$M(t) = E_b\, I_b\, \kappa(t) \qquad \text{(VI.34)}$$

Substituting equation (VI.34) into (VI.10), (VI.17), and (VI.22) leads to three different expressions for the time dependent PZT voltage.

VII. Results

In this section the analytical models developed using the engineering software program MATLAB with the experimental results obtained in Ref [8] will be verified. This verification will be performed in order to test the validity and accuracy of the analytical model of the cantilever beam with piezoelectric material. After the validation of the analytical results with the experimental ones different case studies will be performed to investigate the effect of varies parameters on obtaining maximum output power from the piezoelectric material used as a sensor.

- The three signals with a phase shift of 90 degrees which coincides with the phase shift measured by the impedance analyzer, see Fig. 19.
- The voltage calculated from both the Pin-force and Enhanced pin-force methods are nearly coincident see Fig. 23. This is because in case of the pin-force method we assume constant strain through the PZT while in case of the Enhanced pin-force method considers an increasing linear strain through the PZT, but in fact the PZT is so thin so the linear increase of the strain is negligible and the two results are the same.
- The Euler Bernoulli method produces a voltage that is more than half the other two voltages, see Fig. 22, and 23. This is because this method does not assume that the PZT bends on its own neutral axis.
- The Euler Bernoulli is shifted 180 degrees. This is because the negative sign in the moment equation.

The power is calculated for the three methods, see Fig. 22. To generate maximum power, the load impedance is set equal to the internal PZT impedance, see Fig. 29. Only the steady state portion of the response is used. The power values will be less if the transient response is utilized. This is because the voltage signal has not reached its maximum magnitude.

The equation used to calculate power from an AC voltage signal is:

$$P = \sum V_s^2\,(t_i).R_L / (R_L + R_s)^2.n \qquad \text{(VI.35)}$$

Where V_S is the source voltage, and n is the number of time steps.

The power produced using the Euler Bernoulli method is lower than the other two values of power, see Fig. 24and 25. This is because the Euler Bernoulli method is correctly assuming that the PZT does not bend on its own neutral axis but bends on another shifted neutral axis. By utilizing the optimized variables of PZT location, PZT length, Thickness ratio, and Forcing function location, the power produced using the Euler Bernoulli method is increased over 15000 % as shown in Fig.27, and Table 2.

VIII. Conclusion

Design a complete system to detect the Aircraft at touchdown depends mainly on the sensing elements, how and where they are distributed on the structures so that they can produce maximum output voltage and power. The results of the analytical models developed using the engineering software program MATLAB are satisfactory agreed with the experimental results obtained in Ref [8]. These results showed that the power produced using the Euler Bernoulli method is lower than the values of power of the other two methods, since the Euler Bernoulli method is correctly assuming that PZT does not bend on its own neutral axis but bends on another shifted neutral axis. By utilizing the optimized variables, PZT location, PZT length, thickness ratio, and the location of the forcing function, we obtained a maximum power values. Also to generate maximum power, the load impedance is set equal to the internal PZT impedance. It is recommended while calculating the output power, to consider the steady state portion of the response only, otherwise the power values will be less if the transient response is utilized, since the voltage signal has not reached its maximum magnitude.

IX- Control Design for Future Work

The smart structure as mentioned before involves four key elements; actuators, sensors, control strategies, and power conditioning electronics. From point of view of control, the block diagram is as shown in Fig.28.

In this research, it will be recommended using the piezoelectric sensing elements within the elevating system of the aircraft to measure the descending rate so as to control the rate of descending and consequently avoiding heavy landing. We have to point out the following comments:

a-The relationship between descending rate and output voltage of the sensor seems to be a nonlinear relation that can be linearized at certain operating condition. In this case minimization of the descending angle θ is required.

b-The power electronic unit will be assort of a power amplifier with transfer function K (s) = k1 (conditionally linear element).

c-The actuator is a position control servo-system that must ensure zero steady state error. In other words it must of type 1 see Ref [13], [14].

Thus the block diagram in this case will be as shown in Fig. 29.

The transfer function (TF) of the plant G(s) is the multiplication of the (TF) of the power electronics by the (TF) of the actuator which may result of the following form,

$$G(s) = \frac{K}{S(a_n s^n + \ldots.. + a_1 s + a_0)} \qquad \text{(IX.1)}$$

In this case n may be reduced by well known different reduction techniques Ref [12]. Suitable value of n = 2 was found to be convenient in tracking systems Ref [14].

a- The maximum controller output must be bounded to a certain limited value to permit linearity of the power electronic unit
b- Disturbances imbedded to the plant (i.e. between the power electronic unit and actuator) are ineffective since the complement of the circuit is of type 1 Ref [14].
c- The block diagram shown in Fig. 29, in a non-unity feedback control system, in other words it is a non standard form to let the method of inequalities Ref [15] be applicable.
It is found that it was appropriate to apply optimum coordination approach Ref [16] to find out a simple cascade controller and a proportional feedback controller. This approach Ref [16] had been awarded at the 1987 IEEE-SMC conference at the Radison Mark Plaza Hotel, Alexandria, Virginia, Oct 20-23, 1987. Finding out the viable performance specifications, and applying the optimal coordination approach the given problem will be the subject of the future work of the authers.

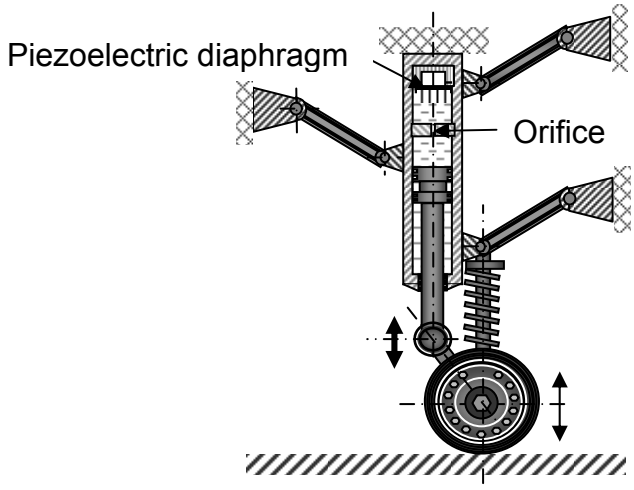

Fig. 1, An Example of the landing gear of light weight training Aircraft with assembled piezoelectric sensor.

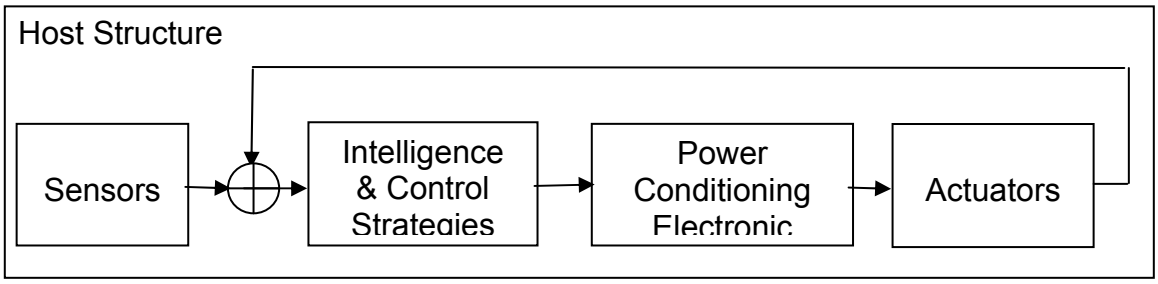

Fig. 2, Smart structure system with it's four basic key elements.

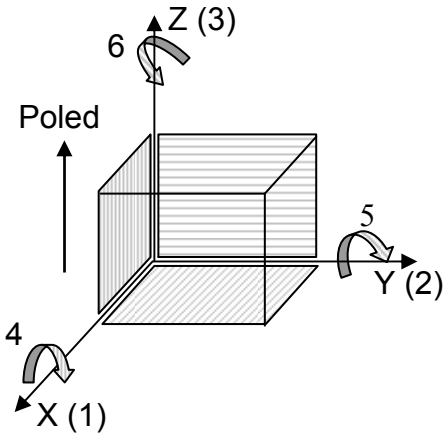

Fig. 3, Constant axis numbering scheme.

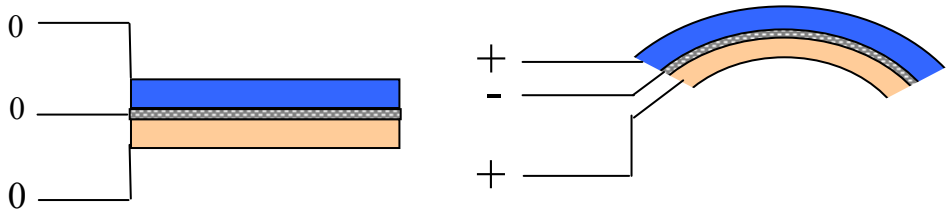

Fig. 4, Piezoelectric bender before and after applying field between the inner and outer electrode

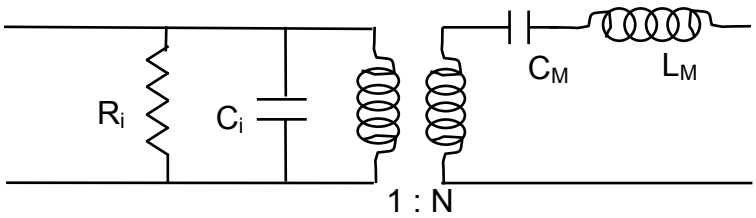

Fig. 5, Simplified piezoelectric element equivalent circuit

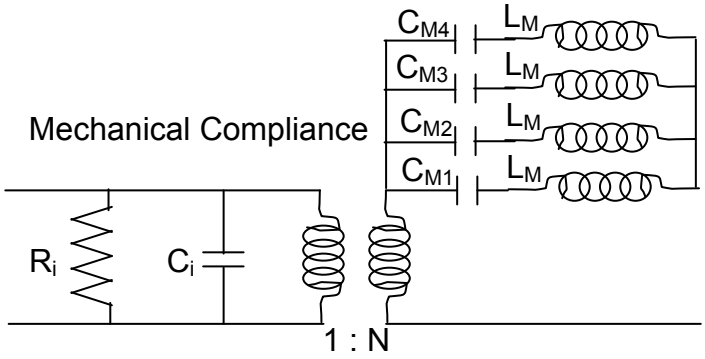

Fig. 6, Mechanical compliance C_M for many resonant modes in the transformers.

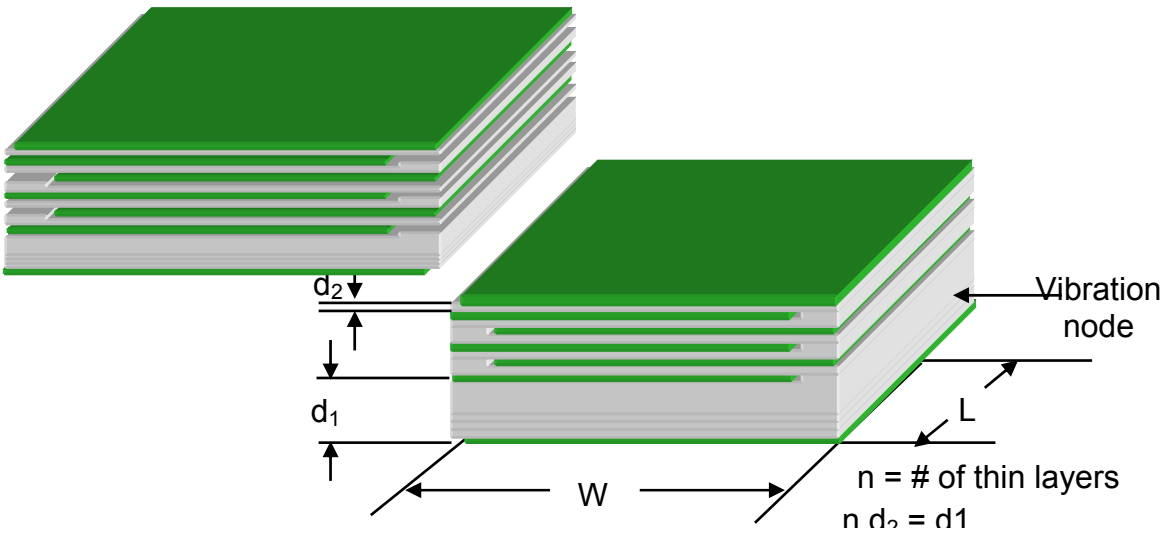

Fig. 7, Simple Stack Piezoelectric Transformer.

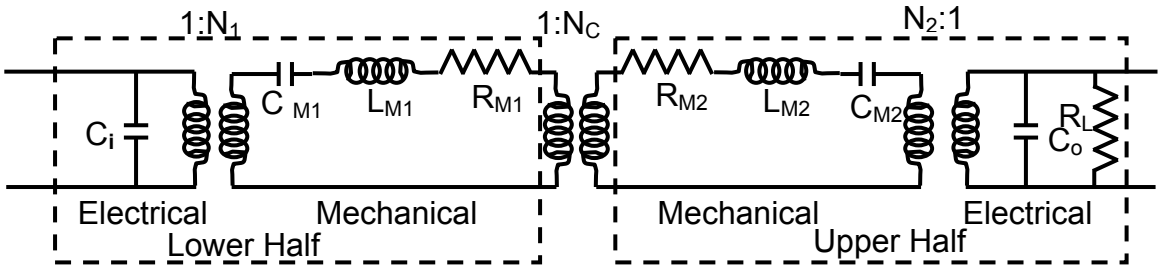

Fig. 8, Equivalent circuit model for the transformer.

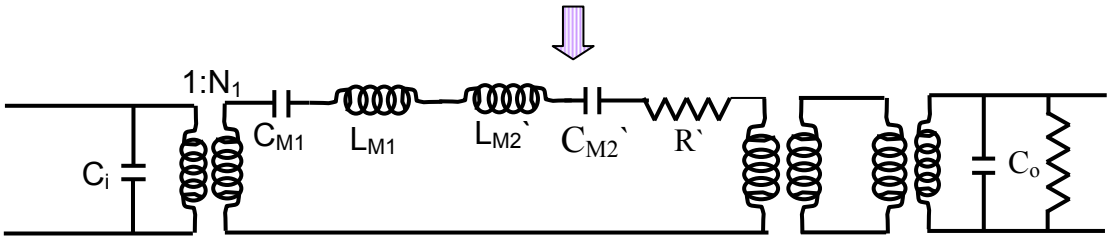

Fig. 9, Equivalent circuit model for the transformer.

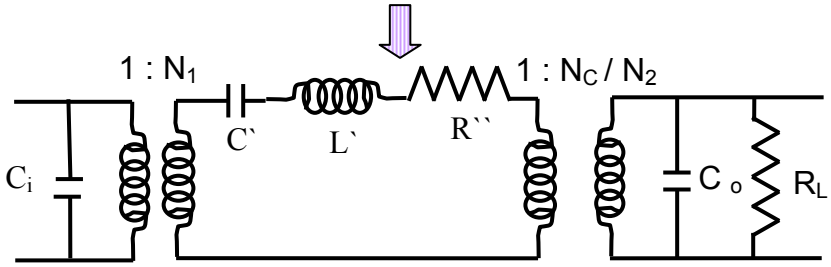

Fig. 10, Second level simplification for the equivalent circuit of the transformer

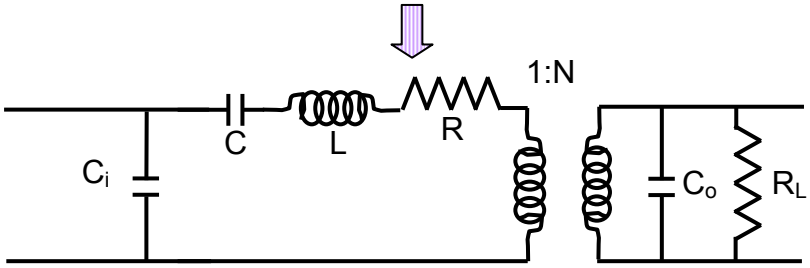

Fig. 11, Final simplification of the equivalent circuit model for the transformer.

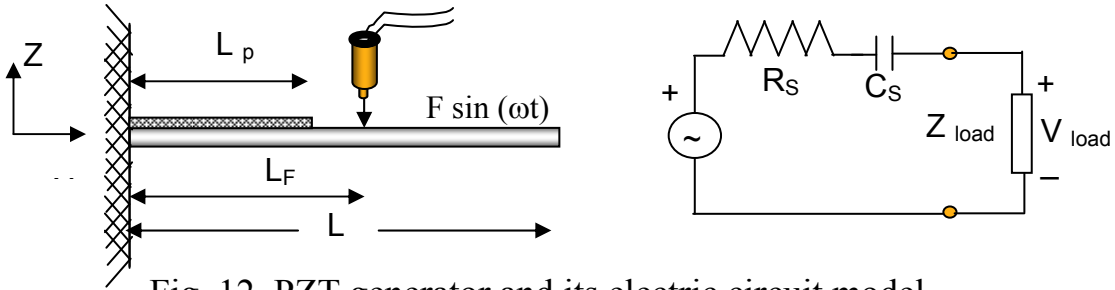

Fig. 12, PZT generator and its electric circuit model

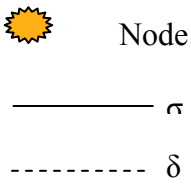

Frequency	Wave Length
ω_o	$\lambda / 2$
$2\ \omega_o$	λ
$3\ \omega_o$	$3\ \lambda / 2$

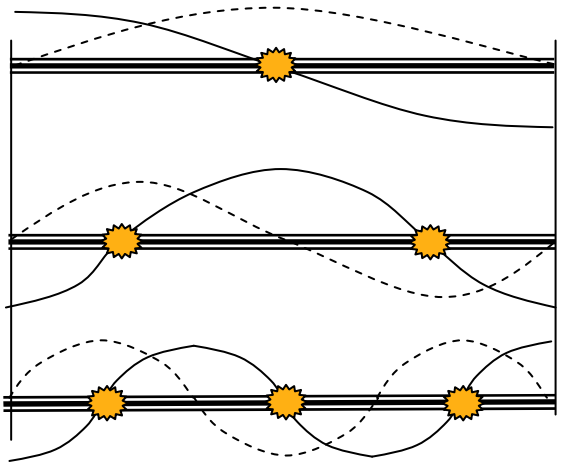

Fig. 13, Nodes of the transformer when driven at harmonic frequencies.

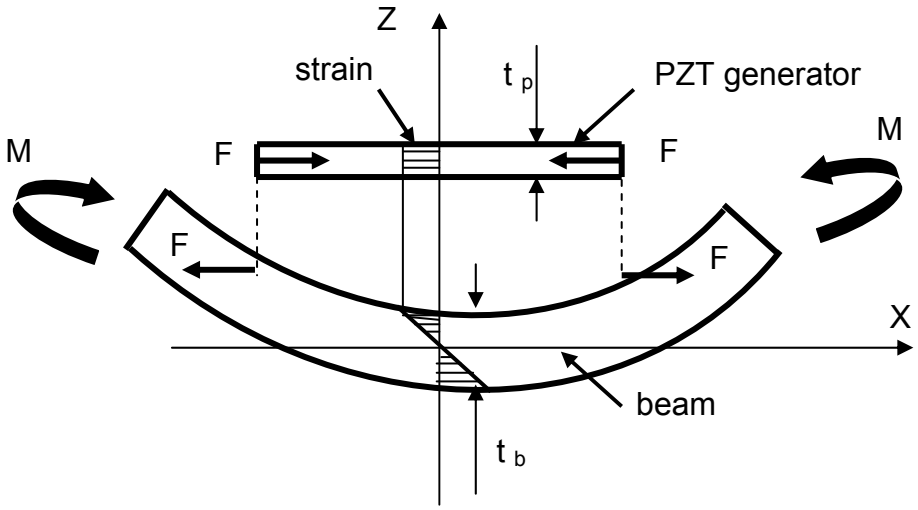

Fig. 14, The pin-force model of unimorph PZT and substrate

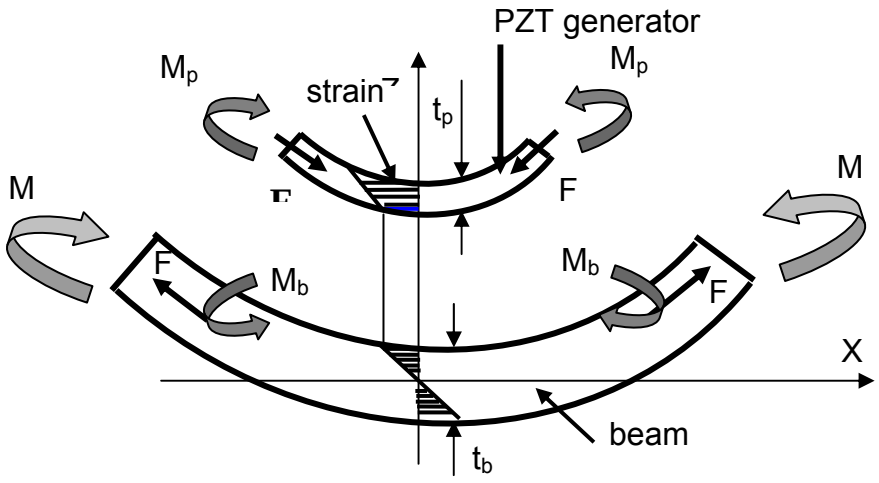

Fig. 15, The enhanced pin-force model of unimorph PZT and substrate

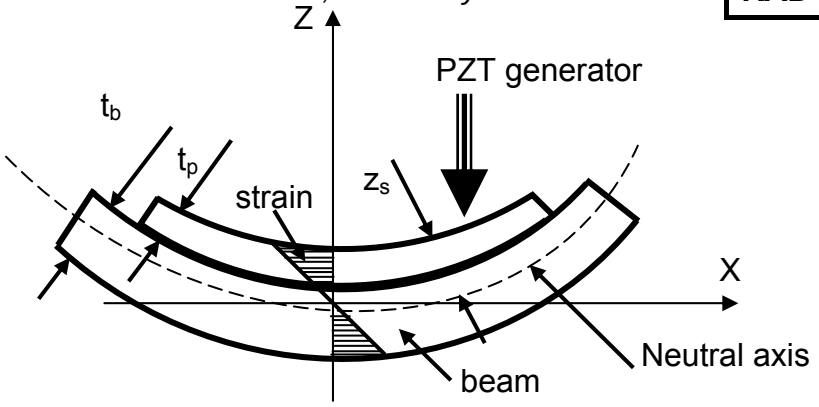

Fig. 16-a, Euler-Bernoulli model of PZT and substrate

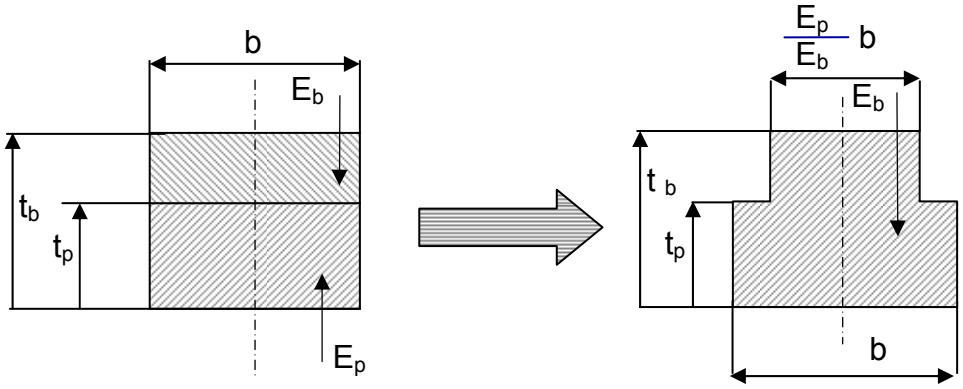

Fig. 16-b, Euler-Bernoulli model along with the modulus-weighted neutral axis.

Sample of MATLAB Results

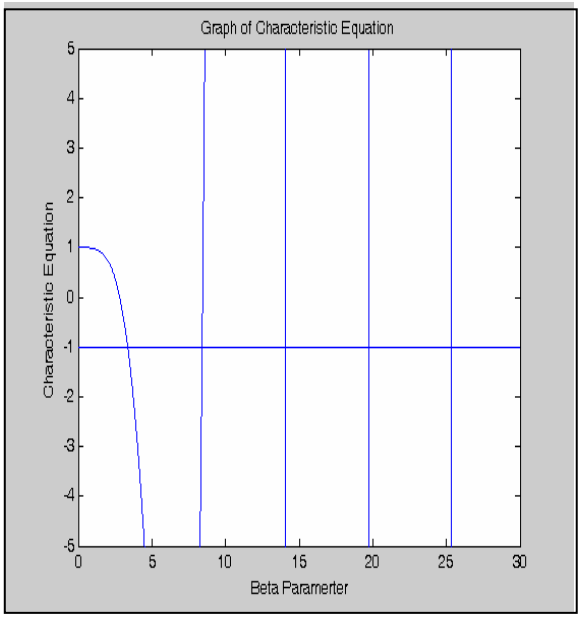

Fig. 17, The first five natural frequencies

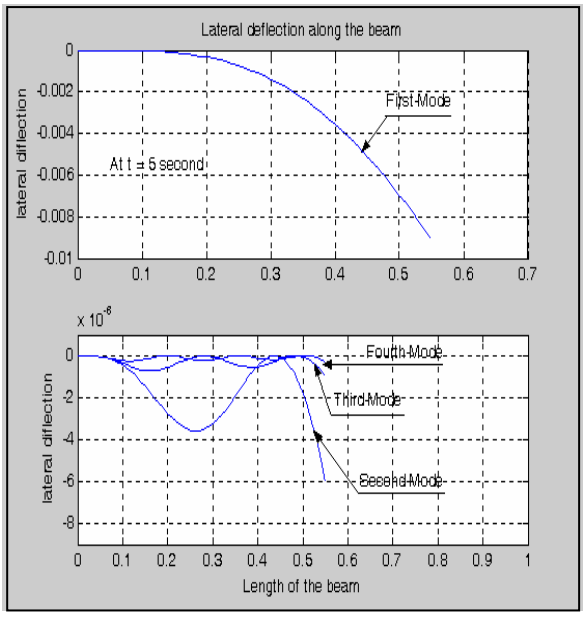

Fig. 18-a, First four mode shapes of the beam

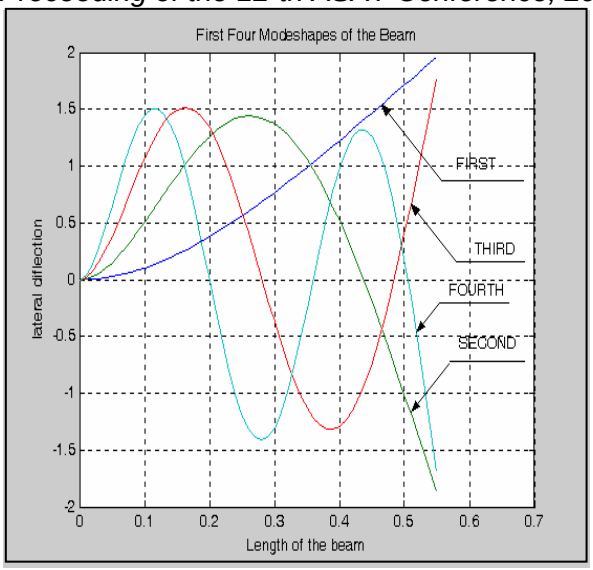

Fig. 18-b, First four mode shapes of the beam

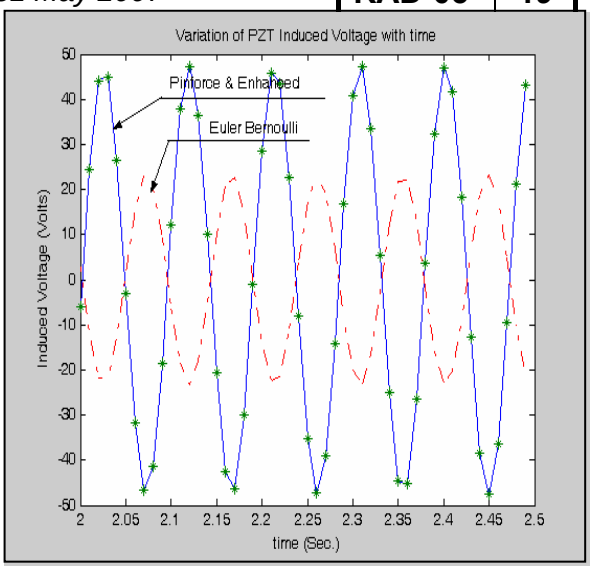

Fig. 19, PZT voltages calculated from analytical beam model

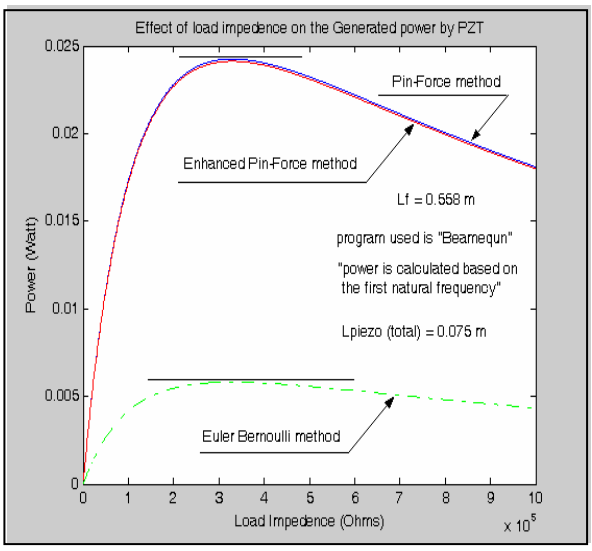

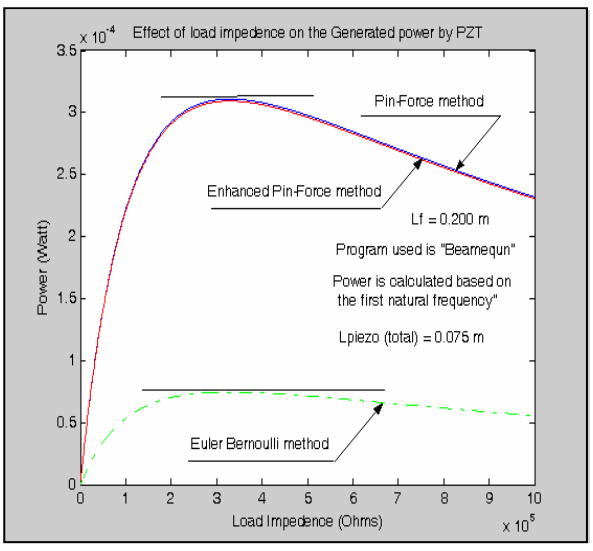

Fig. 20, Effect of load impedance on the Generated power by PZT

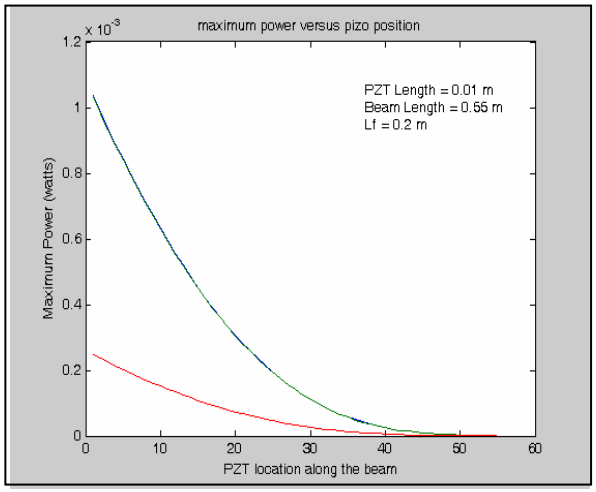

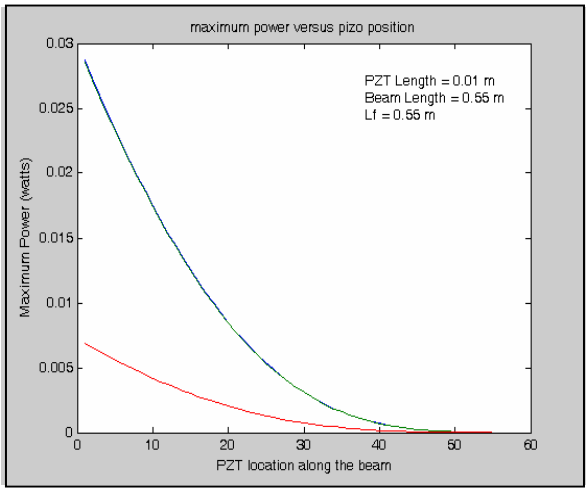

Fig. 21, Power output of the three methods versus the different positions of the PZT along the beam.

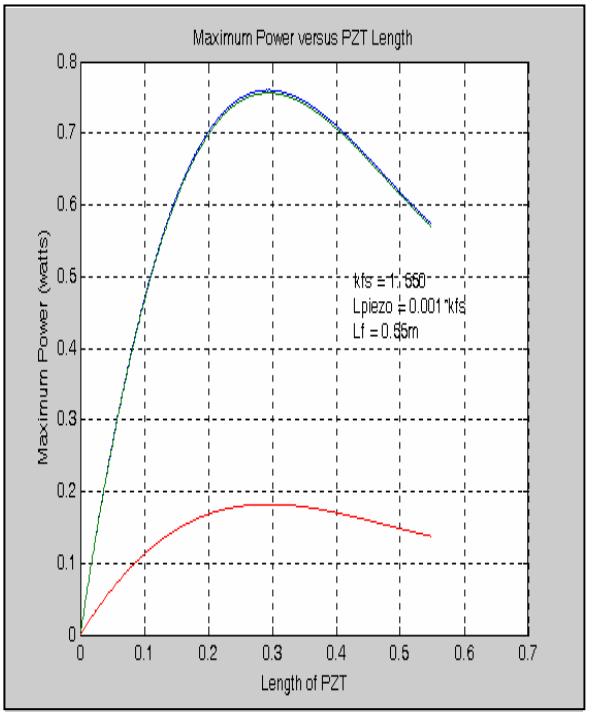

Fig. 22, Maximum output power versus PZT length.

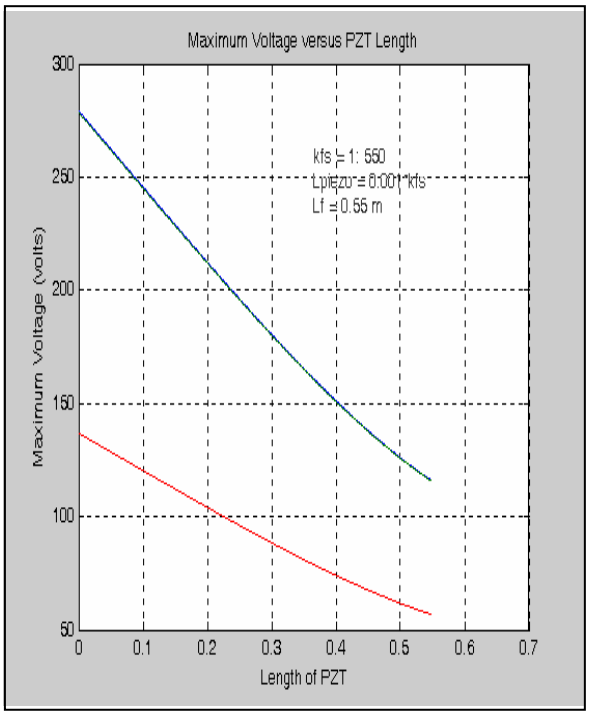

Fig. 23, Maximum output voltage versus PZT length.

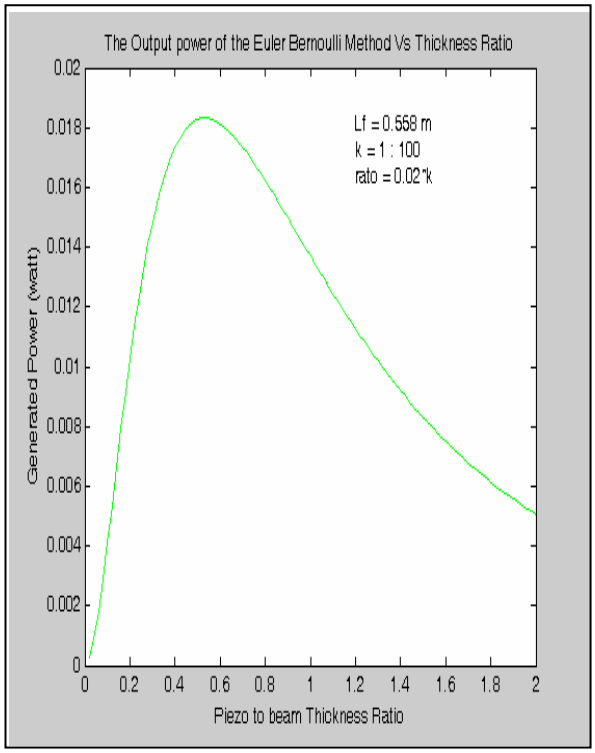

Fig. 24, Maximum output power versus PZT length.

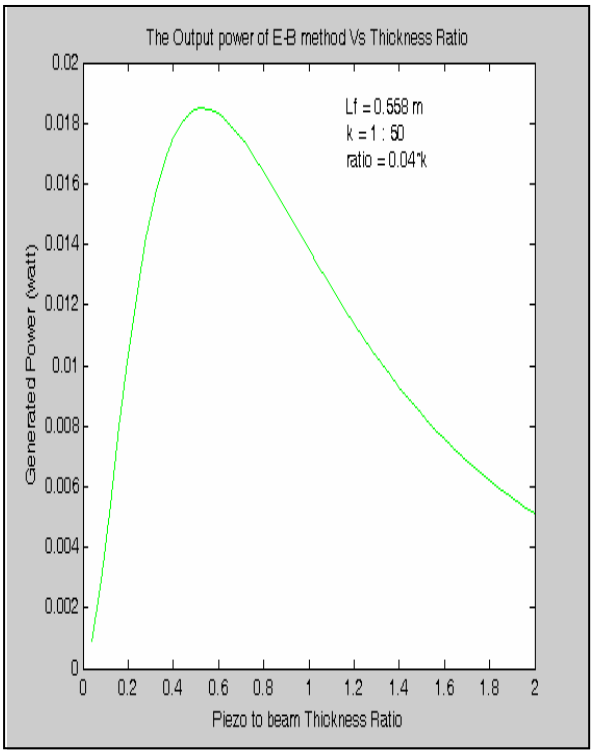

Fig. 25, Maximum output voltage versus PZT length.

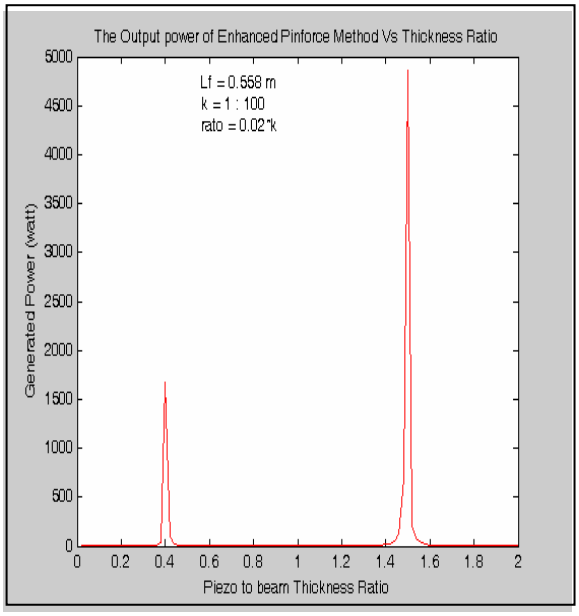

Fig. 26, Power output of the Pin-force method increases exponentially whenever the denominator of the model's equation equals zero

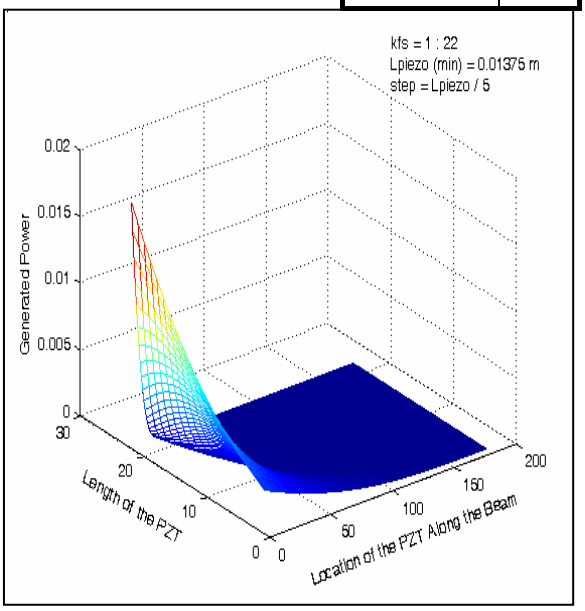

Fig. 27, Output power generated for different PZT lengths at different locations along the beam.

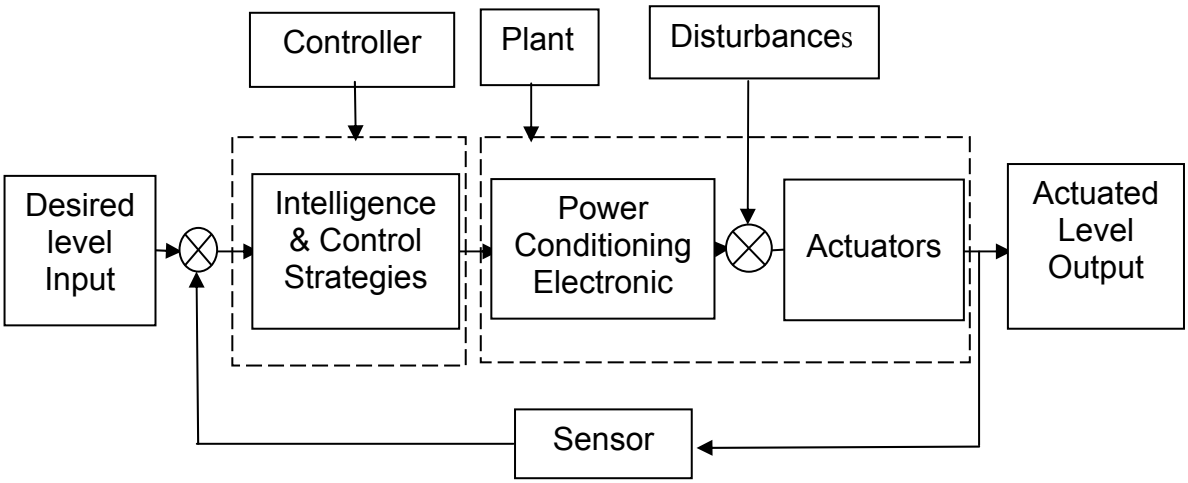

Fig. 28, Block diagram for the control system before simplification.

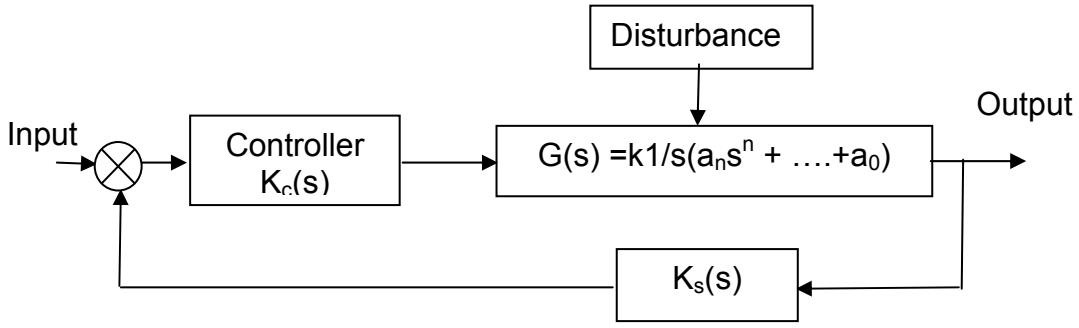

Fig. 29, Simple cascade controller and a proportional feed-back controller.

Table 1. The first five natural frequencies

Natural freq.	Rad/s	Hz
1	66.68	10.612
2	417.87	66.506
3	1170.1	186.22
4	2294	365.1
5	3790.1	603.22

Table 2. A comparison between the power produced from the three methods used

	Method	Power (μ w)		Increase percentage
		Original	Optimized	
1	Pin - force	0.870	2380	270,000 %
2	Enhanced Pin - force	0.866	5365	600,000 %
3	Euler Bernoulli	0.209	33	15,000 %

LITERATURE CITED

[1] Ingerjit Chopra. 2002. Review of State of Art of Smart Structures and Integrated System. AIAA Jurnal. Vol. 40, No. 11, November 2002.
[2] Anand K. Asundi, Director, Sensors and Actuators SRP. School of Mechanical and Production Engineering. Smart Structures Research at NTU. Nanyang Technological University. Singapore
[3] James R. Phillips. Sr.Member of Technical Staff. Piezoelectric Technology Primer.
[4] Wilkie, W.K., et al. Low-Cost Piezocomposite Actuator for Structural Control Applications. Proc. SPIE's 7th Annual International Symposium on Smart Structures and Materials, Newport Beach CA, March 5-9, 2000.
[5] Benjeddou A., Trindade M.A. and Ohayon R. New Shear Actuated Smart Structure Beam Finite Element. AIAA Jurnal. Vol. 37 (3): 378-383, 1999.
[6] Inman, D.J., Engineering Vibration, 2nd edition, Prentic Hall, 2000.
[7] Sirohi, J., and Chopra, I. Fundamental Understanding of Piezoelectric Strain sensors. Journal of Intelligent Material Systems and Structures, Vol.11, April 2000, pp.246-257.
[8] Eggborn, T. 2003. Analytical Models to Predict Power Harvesting with Piezoelectric Materials. For completion of Master of Science in Mechanical Engineering, Virginia Polytechnic Institute and State University.
[9] Abou-Amer S. A. 1991. Control of Panel Flutter at High Supersonic Speed. Submitted in partial fulfillment of requirements for the degree of doctor of philosophy in Mechanical and Aerospace Engineering in the Graduate School of the Illinois Institute of Technology. Chicago, Illinois.
[10] Piezoelectric Technology Primer. James R. Phillips. Sr. Member of Technical Staff. CTS Wireless Components. 4800 Alameda Blvd. N.E.
[11] Electro Ceramics Applications.http://www.morganelectroceramics.com/apps1. html
[12] Dahshan A. M. A., Fawzy A. S., and El Sawy Y. A. 1985. Comparison of Several Model Reduction Techniques. IEEE International Conference on System, Man, and Cybernetics, Nov. 1985. PP. 1029-1033.
[13] Dahshan A. M. A., Aly G. M., and El Singaby M. I. 1989. Design of a Longitudinal Ride Control System for STOL Aircraft Using the Optimal Coordination Approach. IFAC-A/PAC, Nancy, Jul. 3-5, 1989.
[14] Chen C. T. Analysis and Synthesis of Linear Control Systems. New York, HRW series, 1975.
[15] Dahshan A.M. A. 1981. Design of Control Systems by the Method of Inequalities. Ph.D. Thesis. Oct. 1981. UMIST, UK.
[16] Dahshan A. M. A., Fawzy A. S., Aly G. M., and El Singaby M. I. 1986. An Optimal Coordination Approach for Solving Control Problems Using the Method of Inequalities. Proceeding of 1986 IEEE International Conference of System, Man, and Cy bernatics, Nov. Vol. 2, PP 1525-1529.
[17] Austin F., Knowles G. J., Jung W. G., Tung C. C., and Sheedy E. M. 1992. Adaptive/Conformal Wing Design for Future Aircraft. Grumman Corporate Research Center. Paper presented at the 1st European Conf. on Smart Structures and Materials, Glasgow 1992.

[18] Boller C., Honlinger H., Sensburg O. 1992. Technological Challenges with Smart Structures in German Aircraft Industry. MBB-Deutsche Aerospace, Aircraft Dividion, Munchen, Germany.